International Journal of Multiphase Flow 36 (2010) 71–77

Contents lists available at ScienceDirect

International Journal of Multiphase Flow

journal homepage: www.elsevier.com/locate/ijmulflow

Multiscale computations of thin films in multiphase flows

S. Thomas [a,*], A. Esmaeeli [b], G. Tryggvason [a]

[a] Worcester Polytechnic Institute, Worcester, MA 01609, USA
[b] Southern Illinois University—Carbondale, Carbondale, IL 62901, USA

ARTICLE INFO

Article history:
Received 22 January 2009
Received in revised form 8 August 2009
Accepted 9 August 2009
Available online 13 August 2009

Keywords:
Direct numerical simulations
Thin films
Multiscale
Drops
Multiphase flow

ABSTRACT

In multiphase flows thin films are often encountered when fluid masses collide. These films can become very thin and in direct numerical simulations (DNS) it is often impractical to resolve their thickness fully, even with adaptive grid refining. Here we examine the collision of a fluid drop with a wall and develop a multiscale approach to compute the flow in the film between the drop and the wall. By using a semi-analytical model for the flow in the film we capture the evolution of films thinner than the grid spacing reasonably well.

1. Introduction

In spite of the rapid progress in direct numerical simulations (DNS) of complex multiphase flows, real systems provide challenges that still limit the range of situations that can be simulated, even when we limit our studies to systems well described by continuum theories. The problem is, as one might expect, one of scale. Generally the smallest length-scale of the flow has to be resolved by O(10) grid points, and as the number of available grid points increases, the range of scales that can be resolved increases. Current computer power makes it possible to simulate two-fluid systems in domains resolved by several hundred grid points in each spatial direction (for thousands of time steps) and simulations of systems resolved by over 1000^3, or billion grid points, are on the horizon. Simulations of that size obviously offer the opportunities to capture flows whose scales span over two orders to magnitude. This is, however, often not enough. Starting with simulations where what we might call the "dominant small-scales" (see below) are fully resolved, it is frequently found that multiphase flows also can generate much smaller features, consisting of very thin films, filaments, and drops. Frequently there is a clear separation of scales between these "features" and the rest of the flow; usually inertia effects are relatively small for the local evolution at the smallest scales; and in isolation these features are often well described by analytical models. While these features can, in principle, be captured by local, adaptive, grid refinement, doing so increases the complexity of the computations significantly and usually results in greatly increased computational time. Furthermore, since the refinement has to be done in stages, such that the size of adjacent control volumes only differs by a factor of two or so, there are practical limits on how much refinement is possible without using up all the available grid resolution at the smallest scale. Here we suggest a different approach and develop a semi-analytical subgrid model for the flow in a thin film between a drop and wall.

The "dominant small-scale" in many multiphase systems is set by the balance of surface tension, viscosity and inertia. For the breakup of a jet, for example, this scale determines the average droplet size. In most cases this scale corresponds to roughly where the appropriately chosen nondimensional numbers, such as Weber, Capillary, Ohnesorge, and Reynolds, are O(1) (and the key word here is obviously "appropriately"). Unfortunately, however, this is often not the only length-scale that exists and frequently the flow also has much smaller features. Consider, for example, the relatively tame problem of a collision of two droplets that are a few hundred micrometers in diameters. As the drops collide, they deform and trap air in a thin film between them. The air drains out of the film and if the drops stay in contact long enough, the film ruptures. It is, however, generally believed that the film thickness must get down to just about few hundred Angstroms before it ruptures. 100 A = 10 nm = 0.01 μm, so if the drops are 500 μm in diameter, the range of scales, from the thickness of the film to the diameter of the drop is $O(10^4)$.

In many cases viscous effects dominate over inertia, and surface tension effects are sufficiently strong to keep the geometry simple. Thus, the flow can often be described analytically and by using the analytical solution it is possible to avoid resolving the small-scale feature. This approach is perhaps best demonstrated by the

* Corresponding author. Tel.: +1 508 615 3499.
E-mail addresses: siju@wpi.edu, sijuthomas@gmail.com (S. Thomas).

0301-9322/$ - see front matter © 2009 Elsevier Ltd. All rights reserved.
doi:10.1016/j.ijmultiphaseflow.2009.08.002

point-particle approximations. For drops much smaller than the smallest flow scales several investigators have carried out simulations where the flow away from the drops is fully resolved but the drops are approximated as point-particles. In the limit of small Reynolds number the drag on the drop can be found analytically and at larger Reynolds numbers the force can often be included using empirical correlations. While adaptive grid refinement could in some cases also be used to capture such small-scale features, the difference in scale often makes that approach impractical. Simulations of multiphase flows containing small bubbles, drops or particles modeled as point-particles go back many years (see Chapter 9 in Prosperetti and Tryggvason, 2007, for a review), but here we are concerned with situations where such models are used in simulations where "most" of the flow is captured fully using DNS. Examples include the computations of bubbles in slurry bubble reactors by Deen et al. (2004), where small catalytic particles are included as point-particles and simulations of atomization where very small droplets are replaced by point-particles (Tomar et al., 2009). Thin films offer another obvious opportunity to include analytical (or quasi-analytical) models of small-scale features. Studies of thin films have a long history and model equations have been developed for a wide range of conditions but so far little has been done to incorporate these models into simulations of the larger scale motion. See, however, the study of Davis et al. (1989) where a thin film model was coupled with a boundary integral computation to examine the collision of drops, as well as the microlayer model for nucleate boiling introduced by Son and Dhir (1998).

The importance of capturing the evolution of thin films near a solid wall accurately is best introduced by an example. Fig. 1 shows a simulation of a drop immersed in a less viscous fluid, released above a sloping wall. The drop density and viscosity are ten times higher than the ambient fluid and the slope of the wall is 45 deg, so the components of the gravity vector perpendicular and parallel to the wall are equal. The properties of the fluids and the computational setup are given in Section 4. The figure shows five frames from the simulation, starting with the initial conditions. The drop falls onto the wall and then slides along it, riding on a thin lubricating layer of the ambient fluid. The drop motion has been computed using three different grid resolutions, with 64, 128, and 192 grid points across the vertical dimension of a domain that is twice the drop diameter. The 64 grid has evenly spaced grid points, but for the finer grids the points are unevenly spaced in the vertical direction in such a way that the resolution near the wall is almost six times as fine as near the top of the domain. The generation of the unevenly spaced grid is a two step process: first we set the grid spacing to be uniform for the bottom one-third of the domain and increasing linearly from there to the top boundary. In the second step we apply a simple Laplacian smoothing several times to make the expansion more gradual. The minimum grid size, near the bottom wall, was 0.003348 for the 128 grid and 0.002232 for the 192 grid. The results from the two finest resolutions are identical, suggesting that both the drop and the lubrication film are fully resolved. Details of the flow in the film are shown in Fig. 2, where the velocity in a small section of the film is shown at the same time as in frame three in Fig. 1. The results are from the computation using the finest grid and there are about eight grid points across the film, showing the linear velocity profile clearly. For the drop resolved on the coarsest grid there is no grid point in the thin film. The grid spacing used to resolve the flow in the thin film is much higher then what is needed to resolve the drop itself. We have repeated this simulation using a full-slip wall, where resolving the film fully is not critical, and find that the drop motion is essentially fully converged on a grid with only half the number of points used for the coarsest grid. For a solid, no-slip wall, the outcome of a simulation with too few grid points in the film is very different as Fig. 1 shows. Not only is the drop shape different, but the poorly resolved drop lags behind the fully resolved one. In Fig. 3 we plot the

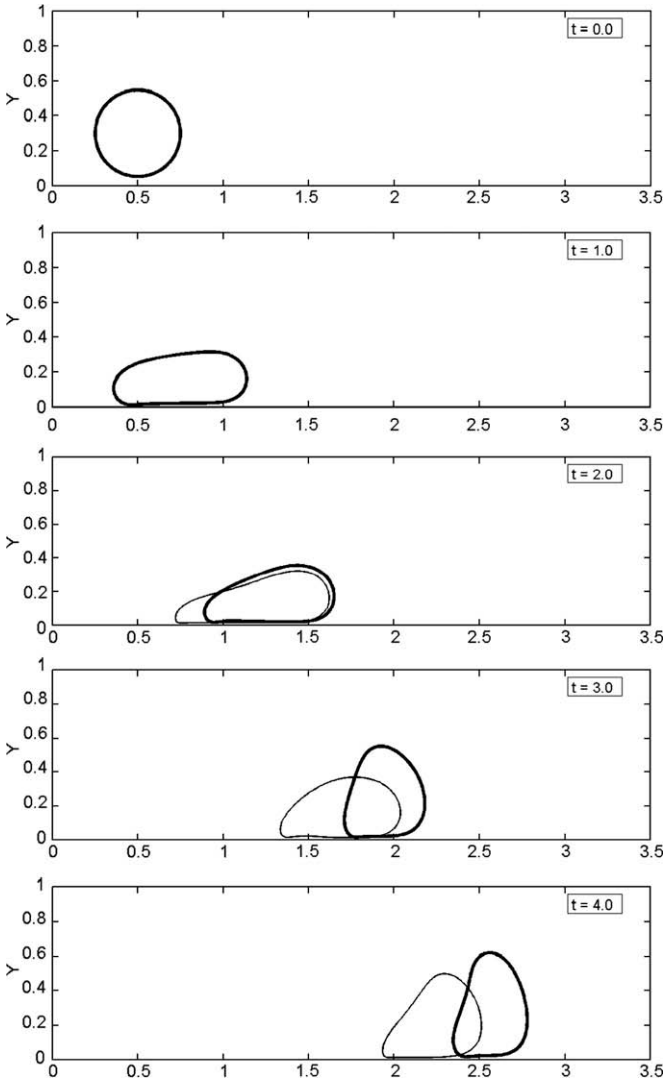

Fig. 1. The motion of a drop falling down a wall with a 45 deg slope, computed using three different resolutions as described in the text. The thick line is fully converged results computed on two fine stretched grids. The results shown by a thin line are computed on a coarse uniform grid. Here, $Eo = 7.955$, $Oh = 0.1414$, and $r = m = 10$.

location of the drop centroid versus time (top) and the minimum thickness of the film (bottom). The drop initially is at rest so it takes it a little while to accelerate but then it slides down the wall with a nearly constant velocity, although there is a slight change in the velocity around time 2.5, presumably corresponding to the change in shape seen between frame three and four in Fig. 1. The drop with the poorly resolved film moves significantly slower than the better resolved ones, as was already seen in Fig. 1. The minimum thickness of the film is well predicted by the finer stretched grids. The thickness is reduced as the drop falls to the wall, then it rebounds slightly around time 2 and eventually the film thickness becomes approximately constant. On the coarse uniform grid, however, the film behaves differently. It does not become as thin as on the finer grids and thus does not rebound nor reach the correct thickness at later times. We have also run the simulation on a 64 grid-points stretched grid, with results similar to those on the finer grids and on a 32 grid-point uniform grid where the differences with the fully resolve solution become even greater than on the 64 grid-point uniform grid.

These results suggest that it would be possible to obtain the correct results using relatively coarse grids by refining them near

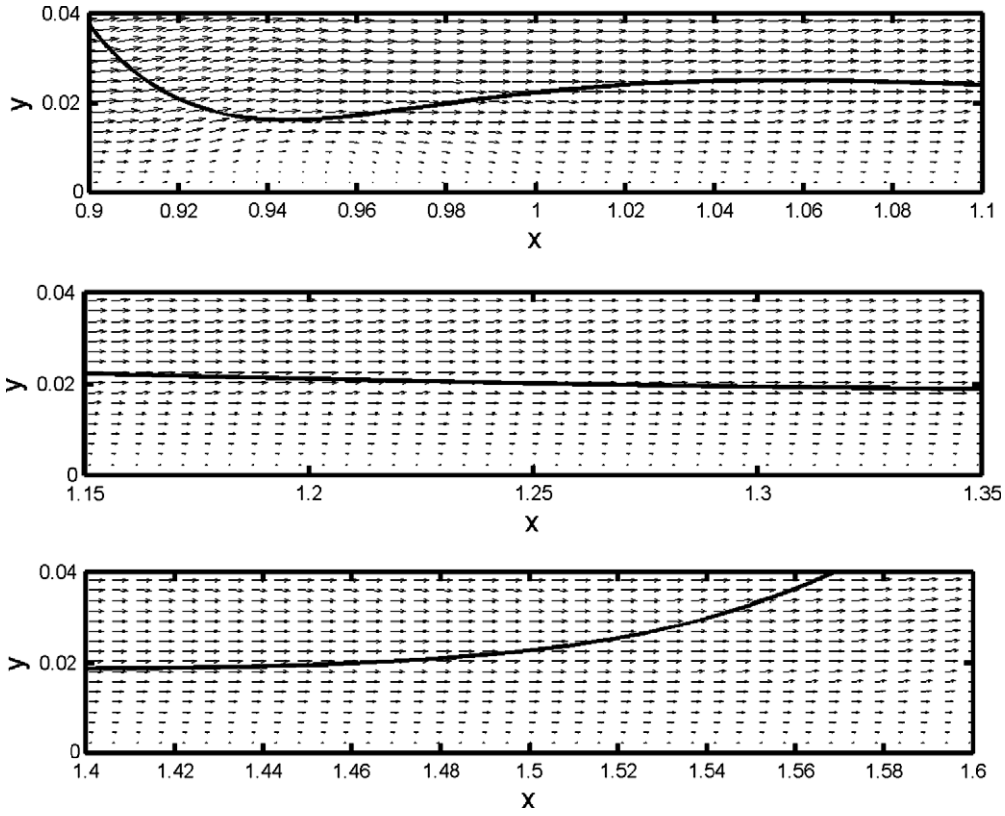

Fig. 2. The flow in the thin film, corresponding to the third frame in Fig. 1, as computed on the finest grid. The top frame shows the flow near the back of the drop, the middle frame shows the flow in the middle and the bottom frame shows the flow near the front.

the wall only. Finer grids do however result in smaller time steps for explicit codes. This, coupled with the simplicity of the flow in the film, suggest that there is an opportunity to capture the behavior near the wall using a wall-layer model based on thin-layer or lubrication theories. The effect of the layer, as obtained in that way, should be fed into the computations of the rest of the motion as a modified boundary condition on the bottom wall. In Section 3 we derive such a model.

2. Numerical method and problem setup

The simulations discussed in this paper are done using a front-tracking/finite-volume method where the governing equations are solved on a fixed, regular, mesh, covering both the ambient fluid and the drop. The interface is marked by connected marker points that are advected with the fluid velocity and a marker function, constructed from the location of the interface, is used to set the density and viscosity of the different fluids. The marker points are also used to compute the surface tension. The method has been used earlier for a large number of simulations of multiphase flows, and both the code and various validation tests have been described in detail in several publications, see Tryggvason et al. (2001), Bunner and Tryggvason (2002), and Esmaeeli and Tryggvason (2005), for example. For applications to problems involving drops, see Nobari and Tryggvason (1996) and Han and Tryggvason (2001).

For the situation simulated here, shown in Fig. 1, the governing nondimensional numbers are the Eötvös number $Eo = \Delta\rho g d^2/\sigma$, the Ohnesorge number $Oh = \mu_d/\sqrt{\rho_d d\sigma}$ and the ratios of the densities $r = \rho_d/\rho_o$ and the viscosities $m = \mu_d/\mu_o$. Here the subscript d refers to the drop and o to the ambient fluid, g is the gravity acceleration, ρ is the density, $\Delta\rho = \rho_d - \rho_o$, μ is the viscosity, σ is the surface tension and d is the drop diameter. The computational domain has a full-slip top and is periodic in the flow-direction. Its height is two drop diameters and the length is seven drop diameters. We have repeated some of the simulations in a larger domain and confirmed that the size of the domain is sufficiently large that it does not influence the results. Here we only do the computations for two-dimensional domains. As discussed briefly later, we believe that extending the approach to three-dimensional flow is relatively straightforward.

3. Modeling the film between a liquid drop and a solid wall

To develop a semi-analytical model of the film trapped between the drop and the wall, we consider the situation sketched in Fig. 4. Gravity pushes the drop toward the wall but the fluid in the film between the drop and the wall takes a finite time to drain so the drop will not touch the wall. Once the film is thin enough, it may rupture but we will not allow for that possibility here.

Assuming the film to be nearly flat and two-dimensional, mass conservation results in the following equation for the thickness of the film, h:

$$\frac{\partial h}{\partial t} + \frac{\partial F}{\partial x} = 0, \tag{1}$$

where

$$F(x) = \int_0^{h(x)} u(x,y)dy \tag{2}$$

is the net volume flux in the film at location x.

The momentum equation for the velocity parallel to the wall, written for a nearly flat two-dimensional film is

$$\rho_o \frac{\partial u}{\partial t} + \rho_o \frac{\partial u^2}{\partial x} = -\frac{dp}{dx} + \mu_o \frac{\partial^2 u}{\partial y^2}. \tag{3}$$

Here we have ignored the effect of surface tension, which could be taken into account by adding an extra term. Integrating this equation across the film results in:

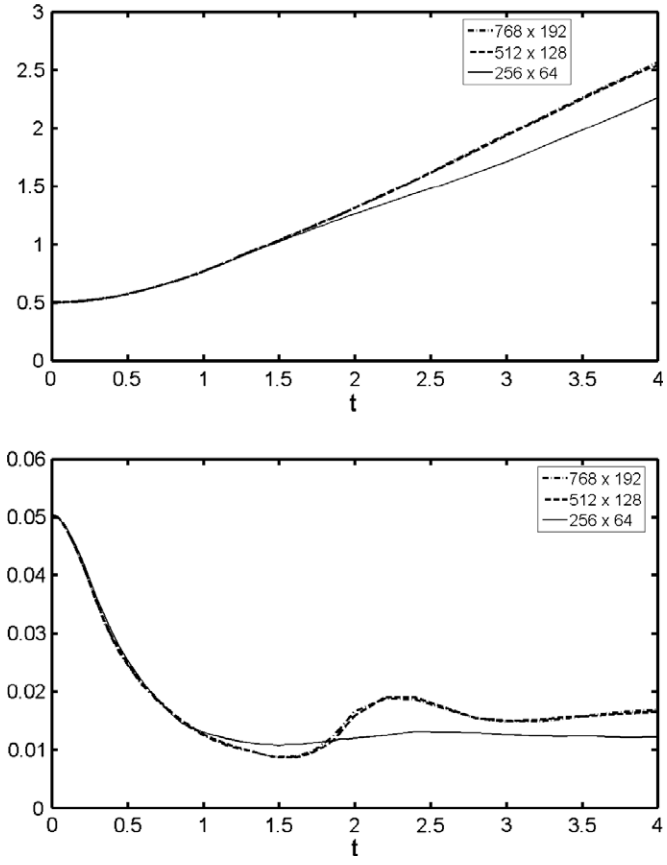

Fig. 3. The location of the drop centroid versus time (top) and the minimum thickness of the film (bottom) for the simulations shown in Fig. 1, computed on two stretched fine grids and a coarse uniform grid.

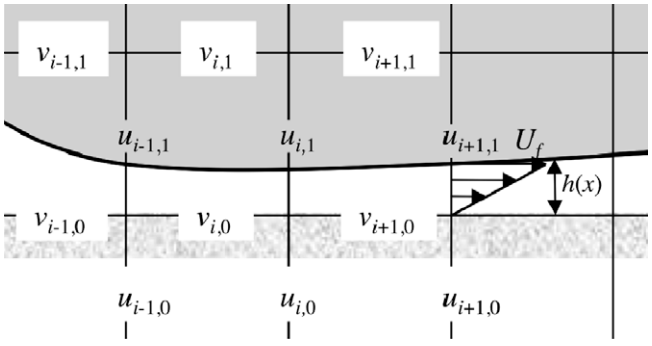

Fig. 4. Schematic showing a thin film between the drop and the wall.

$$\rho_o \frac{\partial F}{\partial t} + \rho_o \frac{\partial M}{\partial x} = -h\left(\frac{dp}{dx}\right)_f + \tau_{h(x)} - \tau_{wall}, \tag{4}$$

where we assume that the pressure gradient is constant across the film. $F(x)$ is defined by Eq. (2) and the momentum flux is

$$M(x) = \int_0^{h(x)} [u(y)]^2 dy. \tag{5}$$

To compute the volume flux F and the momentum flux M, we need to assume a velocity profile $u(y)$. Here we will use the simplest possibility and take the velocity to be linear, going from zero at the wall to, U_f, the velocity of the fluid in the drop at h. Thus,

$$u(y) = U_f \frac{y}{h}; \quad F = \int_0^h u(y)dy = U_f \frac{h}{2}; \quad M = \int_0^h u^2(y)dy = U_f^2 \frac{h}{3},$$

Substituting into Eqs. (1) and (4), yields

$$\begin{aligned} &\frac{\partial h}{\partial t} + \frac{1}{2}\frac{\partial}{\partial x}(hU_f) = 0; \\ &\frac{\partial}{\partial t}(hU_f) + \frac{2}{3}\frac{\partial}{\partial x}(hU_f^2) = -\frac{2h}{\rho_o}\left(\frac{dp}{dx}\right)_f, \end{aligned} \tag{6}$$

where we have used that the shear is constant across the film for a linear velocity profile so that the viscous shear stresses at the wall and the top of the film cancel. Notice that the pressure gradient is assumed to be known (from the solution outside the film). Eqs. (6) allow us to find the thickness of the film $h(x)$ and the fluid velocity at the wall $U_f(x)$, as functions of time.

To discretize these equations we introduce the notation $q = U_f h$. Using a simple explicit first order time integration method and upwinding for the flux terms (assuming positive flow), we can approximate equations (6) by

$$\begin{aligned} h_i^{n+1} &= h_i^n - \frac{\Delta t}{2h}(q_i^n - q_{i-1}^n) \\ q_i^{n+1} &= q_i^n - \frac{2\Delta t}{3h}((q^2/h)_i^n - (q^2/h)_{i-1}^n) - \frac{2h}{\rho_o}\frac{p_{i+1} - p_{i-1}}{2\Delta x}. \end{aligned} \tag{7}$$

Here the pressures are given by the solution of the flow inside the drop, at the top of the film. The linear velocity profile that we have used is likely to work well for clean fluid interfaces where the drop surface is mobile. For more complex problems, such as contaminated surfaces or surfaces where thermocapillary effect are important, it is likely that the velocity profile will have to be more complex. For more sophisticated thin film models see, for example, Oron et al. (1997), Diez et al. (2005), and Kondic and Diez (2005).

Given h and U_f, we can find the wall-shear stress in the film, and by assuming that the stresses are continuous, the shear on the drop surface is given by

$$\tau_f = \mu_o \frac{\partial u}{\partial y} = \mu_o \frac{U_f}{h}. \tag{8}$$

To incorporate the dynamics of the thin film into simulations of the full drop, we assume that the film thickness can be neglected when simulating the drop; that the drop surface coincides with the wall; and that the no-slip conditions are replaced by specifying the wall-shear stress for the portion of the wall where the drop touches it. The pressure at the wall is used to drive the motion in the film (when solving Eq. (7)) and the solution of the film equations is used to give the wall-shear stress where the drop is.

The exact implementation of these equations into a particular numerical method depends on the specifics of the grid used. In our current implementation we use the staggered grid shown in Fig. 4. The velocity is updated at points inside the domain and the ghost points outside the domain are used to set the boundary conditions for the velocity. For points where there is no thin film, the no-slip boundary conditions are enforced by giving the ghost point a velocity such that a linear interpolation for a point on the wall results in the correct wall velocity. Thus, the average of the ghost point velocity and the velocity at the first point inside the domain should be equal to the wall velocity:

$$\frac{u(j=0) + u(j=1)}{2} = U_w, \tag{9}$$

where $U_w = 0$ for a stationary wall. This equation is easily solved for the velocity at the ghost point, $u(j = 0)$.

For points on the wall, where there is a thin film, it is the wall-shear that is given (since we assume that $\tau_w = \tau_f$) and the ghost point velocity must be set in such a way that the slope of the velocity profile at the wall, times the drop viscosity, is equal to the wall-shear:

$$\mu_d \frac{u(j=1)-u(j=0)}{\Delta y} = \tau_f. \tag{10}$$

Knowing the wall-stress we can set the velocity parallel to the wall at the ghost points by:

$$u(j=0) = u(j=1) - \frac{\tau_f \Delta y}{\mu_d}. \tag{11}$$

Thus, to recapitulate, the pressure inside the drop, at the wall, drives the draining of the film through Eq. (7), and given h and U_f the film model determines the velocity boundary conditions for the fluid simulations. Notice that for zero wall-stress (or infinitely high drop viscosity) equation (11) gives full-slip velocity boundary conditions.

To identify whether a grid point belonging to the fixed grid is below a thin film or not, we examine the coordinates of all the front points and for front points that are closer than one grid spacing from the bottom wall, we identify the closest fixed grid points on the wall as belonging to the thin film. When a new point—that was not below a film at the previous time step—is identified, the initial film thickness there is set equal to the grid spacing, Δy, and the thickness is then evolved using the model described above. To simplify the programming, we set the film thickness equal to the grid spacing for all grid points where the thin film model is not being used. Thus, at the edge of the film, when we need the value of h at points outside the film to compute derivatives of h at the last film point, we take this value to be the grid spacing. We have examined the effect of using a different value ($1.2 \times \Delta y$ and $0.8 \times \Delta y$) and found essentially no differences.

The computational procedure is therefore:

1. Identify whether a grid point at a wall belongs to a film or not.
2. For film wall-points, given h and U_f, find the wall-shear τ_f and set the ghost velocities by Eq. (11). For points outside the film, use the no-slip boundary condition (Eq. (9)).
3. Solve the Navier–Stokes equations for the velocity and pressure at the next time step, using the ghost velocities set above.
4. Integrate equations (7), using the pressure at the wall as computed by solving the Navier–Stokes equations (step 3).
5. Go back to (1).

We note that since the film model is solved at the grid points of the fixed grid, and not at the front, extending the model to three-dimensions is straightforward. We simply need to add advection terms in the other spatial direction (say z) to Eqs. (6) and (7) and solve another equation for the momentum flux in the z-direction.

4. Tests

To examine how well the theory outlined above works in practice, we first apply it to the case shown in Figs. 1–3, where we select the governing parameters in such a way that it is possible to resolve the flow in the film on a grid that is reasonably fine, with modest computational effort. In computational units we use, $\rho_d = 2.5$, $\rho_o = 0.25$, $\mu_d = 0.05$, $\mu_o = 0.005$, $\sigma = 0.1$, $g_x = g_y = 1$, and $d = 0.5$, resulting in $Eo = 7.955$, $Oh = 0.1414$, and $r = m = 10$. Fig. 5 shows the drop at the last three times from Fig. 1, when there is a significant difference between the drop resolved on the fine and the coarse grids. We show the fully converged solution from the stretched finest grid, the results from the coarse uniform grid, and then the results from the coarse uniform grid with the model described in the last section used to compute the flow in the film. Although the model results are not identical to the fully converged solution, it is clear that the results are much closer to those, than to the original coarse grid results. This improvement is also seen in Fig. 6, where we plot the location of the centroid (top) and the minimum film thickness (bottom). Here the model results are essentially identical to the fully converged results and much better than the original results from the coarse grid. The deviation between the fully resolved results and those on the coarser grid with the model is likely to be due the simplified nature of the modeling and the assumption of a linear velocity profile (an inaccurate treatment of the endpoint could also lead to a deviation, but as discussed earlier, we have checked that this is not likely). As the grid is refined, the model is activated later and applied to a smaller area (since it is only activated once the interface is less than a grid spacing from the wall) and the difference between the fully resolved results and those utilizing the model are reduced.

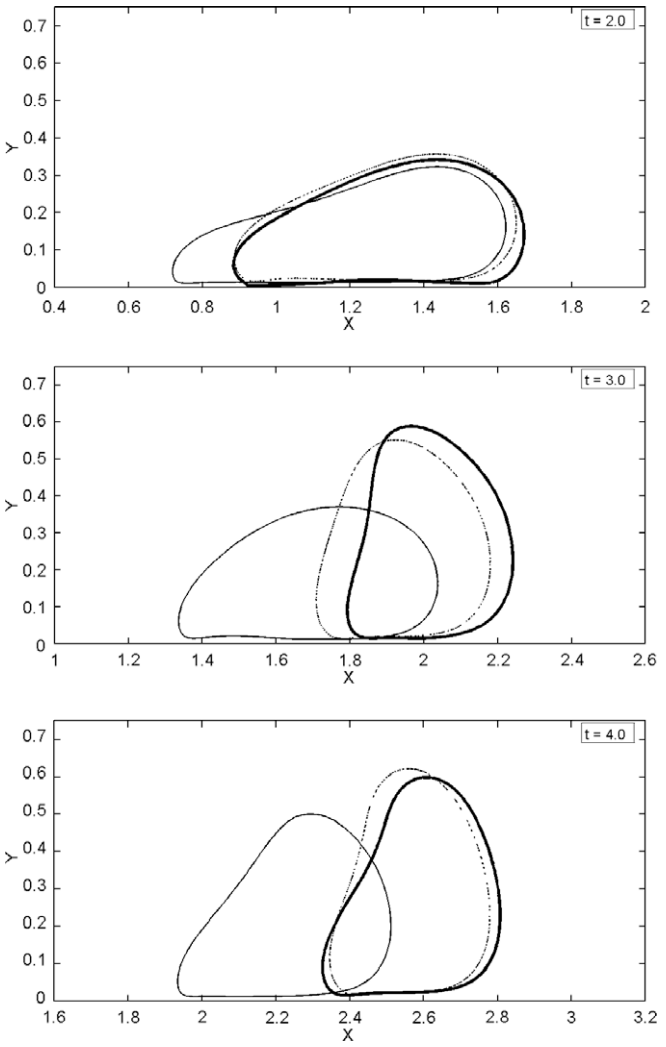

Fig. 5. Comparison of results from simulations on a coarse grid using the wall-film model (dashed line), with direct numerical simulations using the coarse grid without the model (thin line) and the fine stretched grid (thick line) at three times. The coarse grid results with the film model agree reasonably well with the results using the fine grid.

Fig. 7 shows the results of two other tests for different governing parameters, where we compare the results of fully resolved simulations with the results from two simulations on a coarse grid, one with the model and one without. In the top figure the surface tension is sufficiently large so the drop deformation is smaller than in the previous case and in the bottom figure the surface tension is smaller, so the deformation is larger. Specifically, in the top frame we have $Eo = 0.6829$ and $Oh = 0.0253$, and in the bottom frame $Eo = 12.57$ and $Oh = 0.08$. In both cases, $r = m = 10$. For those cases the parameters have been selected such that the film remains

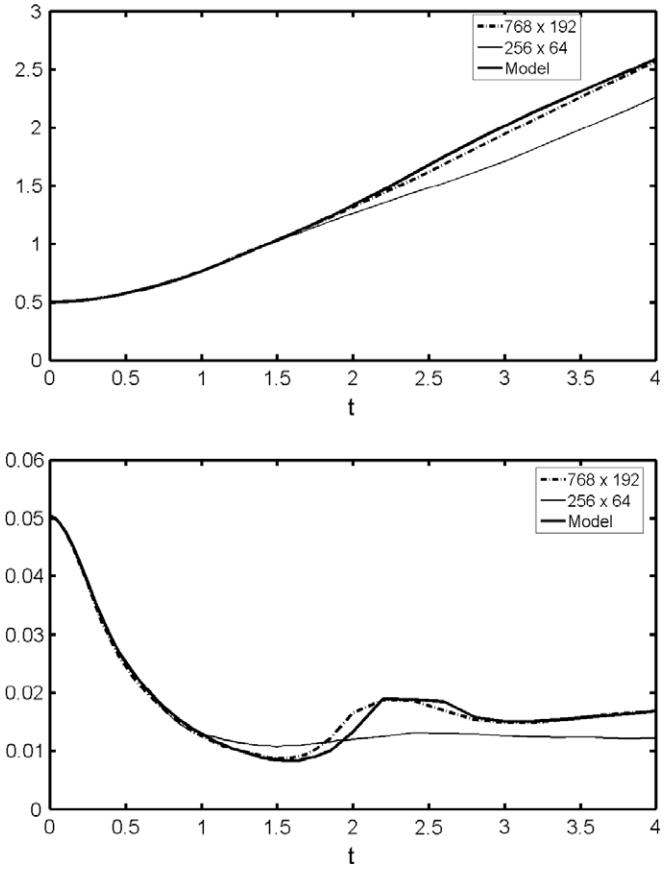

Fig. 6. The location of the centroid of the drop (top) and the minimum thickness of the film near the wall as computed a coarse grid using the wall-film model (dashed line), with direct numerical simulations using the coarse grid without the model (thin line) and the fine stretched grid (thick line) at three times. The coarse grid results with the film model agree reasonably well with the results using the fine grid.

relatively thick, so that it can be resolved relatively easily with non-uniform grid spacing. As for the results presented in Fig. 7, including the model makes the coarse grid results much closer to the fully resolved ones than the results for the coarse grid without the model.

The conditions for the simulation in Figs. 1–3 and 5–7 were selected such that the film between the drop and the wall was relatively thick, and we could therefore fully resolve it on a fine enough grid. The real need for the model is, however, for films that are much thinner. The film will generally become thinner for both less and more deformable drops. For less deformable drops less air is trapped between the drop and the wall and for more deformable drops the film will have more time to drain. In Fig. 8 and Fig. 9 we have increased the gravity acceleration perpendicular to the wall by a factor of four so that the slope of the wall is about 14 deg. The viscosity has also been reduced by 20%. Fig. 8 shows result using the model for a case where the drop is deformable ($\sigma = 0.2$) and in Fig. 9 we simulate a drop with ten times higher surface tension that remains nearly spherical. In the top frames we compare the drop shape as computed on a 64 uniform grid, with and without the model. In the middle frames we plot the location of the centroid versus time and in the bottom frames the evolution of the minimum film thickness is plotted. In both cases we see that there is a significant difference between the results with and without the model. The drop without the model moves significantly slower than when the model is used (b) and the film becomes thinner when the model is used (c). Notice that the film becomes considerable thinner than the minimum grid spacing ($\Delta y = 0.0156$), even when the model is not used. Since the film thickness now becomes much thinner than in the cases shown in Figs. 1–7, we have

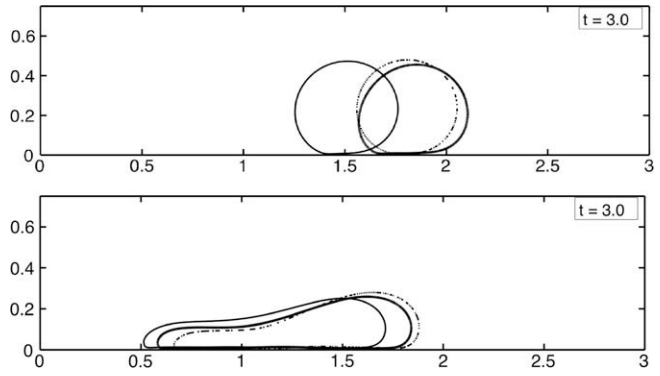

Fig. 7. Comparisons of a nearly spherical (top frame) and a very deformable (bottom frame) drop impacting on a sloping wall. The density and viscosity ratios and the slope of the wall are same as in Figs. 5 and 6, but the *Eo* and *Oh* are different, as listed in the text.

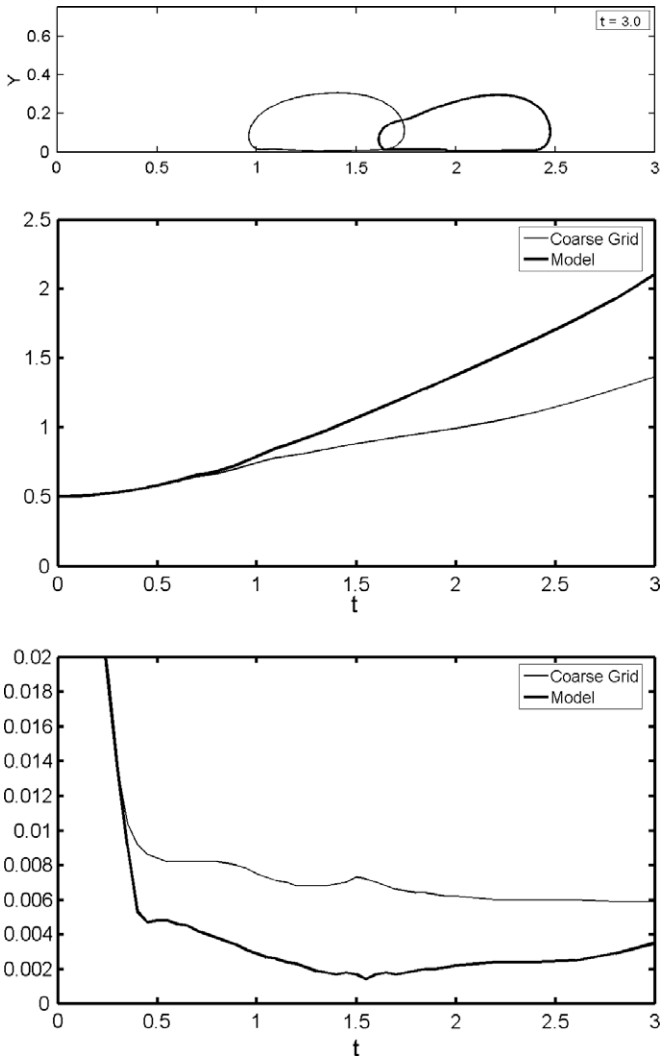

Fig. 8. Motion of a drop computed on a coarse grid with and without the wall-model (top). Location of the centroid of the drop versus time (middle). The minimum thickness of the film near the wall (bottom). The thick line denotes results with the wall-model and the thin line is results without the model.

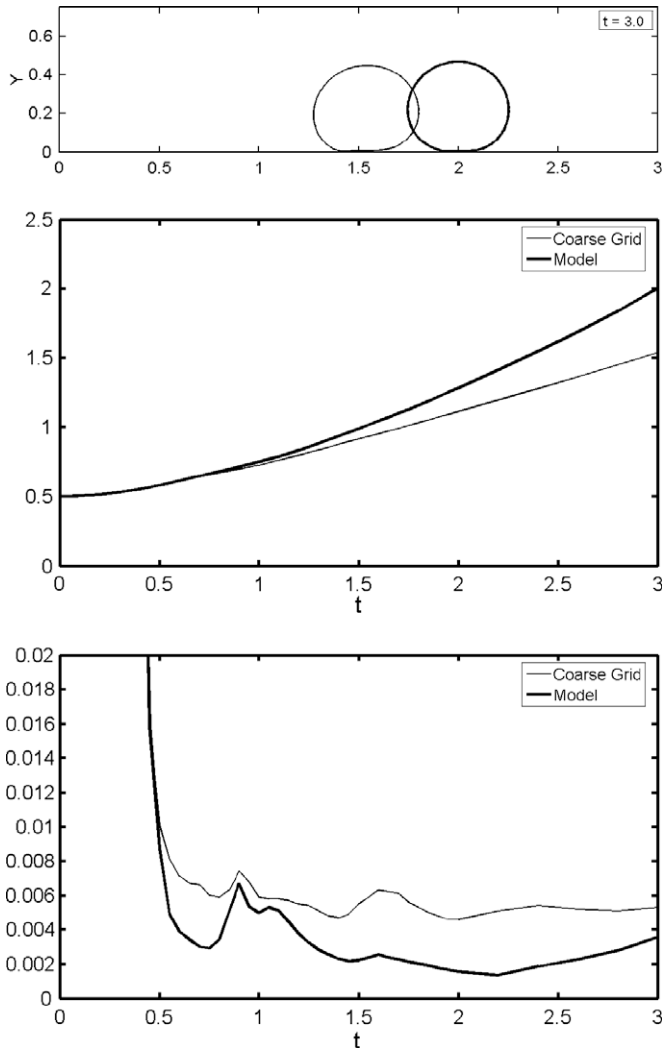

Fig. 9. Motion of a drop computed on a coarse grid with and without the wall-model (top). Location of the centroid of the drop versus time (middle). The minimum thickness of the film near the wall (bottom). The thick line denotes results with the wall-model and the thin line is results without the model.

not attempted to do a grid refinement to obtain a fully converged solution and the purpose of this test is only to show the influence of using the model. However, given the results of the original test case, we expect that using the model will get us much closer to the fully converged solution.

5. Conclusions

We have introduced a method to account for thin films trapped between a drop and a solid wall in front-tracking simulations of multifluid flows, without the need for local adaptive grid refinement. The method is based on solving an equation for the evolution of the film in parallel with computing the fully resolved flow in the rest of the computational domain. The equations governing the evolution of the film are based on standard assumptions used for thin film modeling and use information from the fully resolved part of the domain to drive the film flow. The results from the thin film are, in turn, used to modify the wall-boundary conditions for the fully resolved flow. The model is designed to "kick-in" only when needed (when the film thickness becomes smaller than a grid spacing) and a refinement of the grid used for the fully resolved part of the flow will either delete or eliminate the use of the thin film model automatically. Since the model is activated once the film is thin enough it is, however, possible that too poor of a resolution of the flow outside the film will result in the film never becoming thin enough to activate the model.

For the particular cases examined here, drops moving next to a wall, we expect the importance of modeling the thin film to depend strongly on the specifics of the situation, including the ratios of the density and viscosity and the force driving the drops to the wall. For other situations, such as a bubble sliding along the wall, where the film is essentially stationary, we would expect the effect to be small. Although we have derived and tested the thin film model here for a very specific situation, we expect that the approach is more general and that it can be extended to other situations where thin films form.

As we go to smaller and smaller scales, we eventually reach a point where it is no longer fully justified to assume that the usual continuum hypothesis is accurate. It is then necessary to either change the modeling approach completely by, for example, using molecular simulations or possibly something like the dissipative particle dynamics approach, or work with modified continuum formulations designed to account for small-scale effects. See Werder and co-workers (2005) and Nie et al. (2004) for recent attempts to couple molecular dynamics with continuum simulations.

Acknowledgements

This study was funded in part by NSF Grant CTS-0522581 and NASA Grant NNC04GA75G.

References

Bunner, B., Tryggvason, G., 2002. Dynamics of homogeneous bubbly flows. Part 1: Rise velocity and microstructure of the bubbles. J. Fluid Mech. 466, 17–52.
Davis, R.H., Schonberg, J.A., Rallison, J.M., 1989. The lubrication force between 2 viscous drops. Phys. Fluids A: Fluid Dyn. 1, 77–81.
Deen, N.G., van Sint Annaland, M., Kuipers, J.A.M., 2004. Multi-scale modeling of dispersed gas–liquid two-phase flow. Chem. Eng. Sci. 59, 1853–1861.
Diez, J.A., González, A.G., Gomba, J., Gratton, R., Kondic, L., 2005. Unstable spreading of a fluid filament on a vertical plane: experiments and simulations. Physica D: Nonlinear Phenomena 1–4, 49–61.
Esmaeeli, A., Tryggvason, G., 2005. A direct numerical simulation study of the buoyant rise of bubbles at O(100) Reynolds number. Phys. Fluids 17, 093303.
Han, J., Tryggvason, G., 2001. Secondary breakup of liquid drops in axisymmetric geometry. Part II: Impulsive acceleration. Phys. Fluids 13, 1554–1565.
Kondic, L., Diez, J.A., 2005. On nontrivial traveling waves in thin film flows including contact lines. Physica D: Nonlinear Phenomena 1–4, 135–144.
Nie, X.B., Chen, S.Y., Robbins, W.N.E., Robbins, M.O., 2004. A continuum and molecular dynamics hybrid method for micro and nano-fluid flow. J. Fluid Mech. 500, 55–64.
Nobari, M.R.H., Tryggvason, G., 1996. Numerical simulations of three-dimensional drop collisions. AIAA J. 34, 750–755.
Prosperetti, A., Tryggvason, G., 2007. Computational Methods for Multiphase Flow. Cambridge University Press, Cambridge.
Oron, A., Davis, S.H., Bankoff, G.S., 1997. Long-scale evolution of thin liquid films. Rev. Mod. Phys. 69, 931–980.
Son, G., Dhir, V.K., 1998. Numerical simulation of film boiling near critical pressures with a level set method. J. Heat Transfer: Trans. ASME 120, 183–192.
Tomar, G., Fuster, D., Zaleski, S., Popinet, S., 2009. Multiscale simulations of primary atomization. ICLASS 2009, 11th Triennial International Annual Conference on Liquid Atomization and Spray Systems, Vail, Colorado USA, July 2009.
Tryggvason, G., Bunner, B., Esmaeeli, A., Juric, D., Al-Rawahi, N., Tauber, W., Han, J., Nas, S., Jan, Y.-J., 2001. A front-tracking method for the computations of multiphase flow. J. Comput. Phys. 169, 708–759.
Werder, T., Welther, J.H., Koumoutsakos, P., 2005. Hybrid atomistic–continuum method for the simulation of dense fluid flows. J. Comput. Phys. 205, 373–390.